Computers and Chemical Engineering 33 (2009) 122–132

Contents lists available at ScienceDirect

Computers and Chemical Engineering

journal homepage: www.elsevier.com/locate/compchemeng

Modeling the evaporation of a hydrocarbon feedstock in the convection section of a steam cracker

Sandra C.K. De Schepper, Geraldine J. Heynderickx*, Guy B. Marin

Laboratory for Chemical Technology, Ghent University, Krijgslaan 281 (S5), B-9000 Ghent, Belgium

ARTICLE INFO

Article history:
Received 4 December 2007
Received in revised form 4 July 2008
Accepted 9 July 2008
Available online 5 August 2008

Keywords:
Flow boiling
Two-phase flow
Numerical simulation
VOF
PLIC
CFD

ABSTRACT

A model has been developed allowing to simulate the flow boiling process of a hydrocarbon feedstock. For the calculation of the different horizontal two-phase flow regimes that evolve during flow boiling, use is made of the Volume Of Fluid (VOF) model that uses a Piecewise Linear Interface Calculation (PLIC) method to reconstruct the interface between both phases in each computational cell. In-house developed codes calculate the mass and energy transfer phenomena occurring during this flow boiling process. As such, an existing CFD code is completed with a newly developed complete evaporation model.

The developed model is used to simulate the flow boiling process of a hydrocarbon feedstock in the tubes of a convection section heat exchanger of a steam cracker. The simulation results show a succession of horizontal two-phase flow regimes in agreement with the literature.

1. Introduction

Steam cracking of hydrocarbons is one of the most important processes in petrochemical industry converting a hydrocarbon feedstock into more valuable products such as ethylene and propylene.

A steam-cracking furnace, as can be seen in Fig. 1, consists of two sections: the radiation section and the convection section. The radiation section is heated with burners supplying the necessary heat for the endothermal cracking process. In this section, over 90% of the heat transfer from the flue gas and the furnace walls to the reactor coils is radiative. Hence, the radiation section is an empty volume with at most two rows of vertically suspended tubular reactor coils in the middle of this section. The flue gas flows along these coils. A complete detailed simulation of the radiation section involves a coupled simulation of both the furnace and the reactor coils as the conditions in the reactor coils and the flue gas temperature influence one another (Heynderickx, Oprins, Dick, & Marin, 2001; Stefanidis, Heynderickx, & Marin, 2006).

In the convection section, the remaining energy of the flue gas leaving the radiation section is used to preheat and vaporize the hydrocarbon feedstock and to overheat steam. The hydrocarbon–steam mixture, leaving the convection section, is then introduced in the reactor coils of the radiation section to be cracked. In the convection section, the major part of the heat transfer is due to convection, as the flue gas temperature is much lower. As a result, the convection section is filled with a large number of horizontally suspended heat exchanger tubes over which the flue gas flows. As for the radiation section, a correct simulation of the convection section will require a coupled simulation of the heat transfer from the flue gas side to the heat exchanger tubes and of the phenomena of heating and evaporation inside these tubes.

Comparable to the coking problems in the tubes of the radiation section (Cai, Krzywicki, & Oballa, 2002; Wauters & Marin, 2002), fouling problems can occur in the tubes of the convection section. To analyze and solve these problems, a coupled simulation of the flue gas side and the process gas side of the convection section is needed. Such a simulation can, e.g. reveal the presence of hot spots on the convection section tubes.

The first step in unraveling the convection section coking problem is a correct calculation of the phenomena in the lowest temperature heat exchanger of the convection section where the hydrocarbon feedstock is heated and partially vaporized. Indeed, a correct simulation of this heat exchanger is felt throughout the complete convection section simulation as the different heat exchangers in this section are coupled. Thus, during the flow boiling process, a two-phase vapor–liquid mixture flows through the tubes (Dhir, 1998). The liquid-to-vapor ratio changes continuously, but, even more important, the flow regime of the two-phase mixture changes as well. Although commercial CFD software packages dis-

* Corresponding author. Tel.: +32 926 44516; fax: +32 926 44999.
E-mail address: geraldine.heynderickx@UGent.be (G.J. Heynderickx).

0098-1354/$ – see front matter © 2008 Elsevier Ltd. All rights reserved.
doi:10.1016/j.compchemeng.2008.07.013

Nomenclature

a_i	volumetric interfacial surface area (m^2/m^3)
$C_{1\varepsilon}$	standard k–ε model constant, $C_{1\varepsilon} = 1.44$
$C_{2\varepsilon}$	standard k–ε model constant, $C_{2\varepsilon} = 1.92$
C_p	heat capacity (J/kg K)
C_μ	standard k–ε model constant, $C_\mu = 0.09$
D_H	hydraulic diameter (m)
D_{Sm}	mean Sauter diameter (m)
E	total energy per unit mass (J/kg)
g	gravitational acceleration, $g = 9.81$ m/s^2
H	total enthalpy per unit mass (J/kg)
ΔH	vaporization enthalpy (J/kg)
J	mass flux over the vapor–liquid interface (kg/m^3 s)
J_{lv}	mass transfer from the liquid phase to the vapor phase (kg/m^3 s)
J_{vl}	mass transfer from the vapor phase to the liquid phase (kg/m^3 s)
J'	net mass flux over the vapor–liquid interface (kg/m^2 s)
k	turbulent kinetic energy (J/kg)
Lo	Laplace length (m)
M	molecular weight (kg/kmole)
N_{Lo}	Laplace length number
N_{Re_b}	bubble Reynolds number
N_ρ	density ratio
p	pressure (Pa)
p_{sat}	saturation pressure (Pa)
q_j	conductive heat flux in the x_j-direction (J/m^2 s)
R	universal gas constant (J/mol K)
S_E	source term in the energy equation (J/m^3 s)
S_F	source term in the momentum conservation equation (kg/m^2 s^2)
S_M	source term in the mass conservation equation (kg/m^3 s)
S_{α_k}	source term for volume fraction of phase k (1/s)
T	temperature (K)
T_l	temperature of the liquid phase (K)
T_v	temperature of the vapor phase (K)
T_{sat}	saturation temperature (K)
t	time (s)
u_i	velocity component in the x_i-direction (m/s)
$\bar{u}_i$	Reynolds average of u_i (m/s)
u'_i	Reynolds fluctuation of u_i (m/s)
u_j	velocity component in the x_j-direction (m/s)
$\bar{u}_j$	Reynolds average of u_j (m/s)
u'_j	Reynolds fluctuation of u_j (m/s)
x_i	x_i-direction or coordinate, with i indicating x, y, z (m)
x_j	x_j-direction or coordinate, with j indicating x, y, z (m)

Greek symbols

α_c	accommodation coefficient
α_k	volume fraction of phase k
β_1	mass transfer time relaxation parameter, $\beta_1 = 0.1$ (1/s)
β_2	mass transfer time relaxation parameter, $\beta_2 = 0.1$ (1/s)
δ_{ij}	Kronecker function
ε	void fraction, viscous dissipation of turbulent kinetic energy (m^2/s^3)
μ	dynamic viscosity (Pa s)
μ_k	dynamic viscosity of phase k (Pa s)
μ_{turb}	turbulent viscosity (Pa s)
ν_l	kinematic viscosity of the liquid phase (m^2/s)
ρ	density (kg/m^3)
ρ_k	density of phase k (kg/m^3)
ρ_l	density of the liquid phase (kg/m^3)
ρ_v	density of the vapor phase (kg/m^3)
$\Delta\rho$	density difference (kg/m^3)
σ	surface tension (N/m)
σ_c	condensation coefficient
σ_e	evaporation coefficient
σ_k	standard k–ε model constant, $\sigma_k = 1.00$
σ_ε	standard k–ε model constant, $\sigma_\varepsilon = 1.30$
τ_{ij}	viscous stresses with (i,j) indicating (x,y,z) (kg/m s^2)

pose over several models to simulate the two-phase vapor–liquid flow (Ghorai & Nigam, 2006), it needs to be checked whether the predicted two-phase flow regime corresponds with the actual flow regime for the given liquid-to-vapor ratio. For the commercial CFD software package Fluent Inc. (2006) that has been used in this work, correct results are obtained (De Schepper, Heynderickx, & Marin, 2008). On the other hand, the software package does not dispose over a model that is able to simulate the evaporation process itself. In order to overcome this, an in-house developed code will be used to complete the available CFD code. The results of this work, in particular the phenomena of heat and mass transfer encountered during the flow boiling process in the tubes, are presented in this paper.

2. Flow boiling

Flow boiling inside tubes is a considerably more complex process than pool boiling. The continuous evaporation of liquid results in a vapor volume fraction increase, causing in turn an acceleration of both phases. Flow boiling studies have shown that several flow regimes are observed, depending on the amount of vapor phase that has already been formed (Thome, 2004). Next to inertia, viscous and pressure forces influencing single-phase flow, the

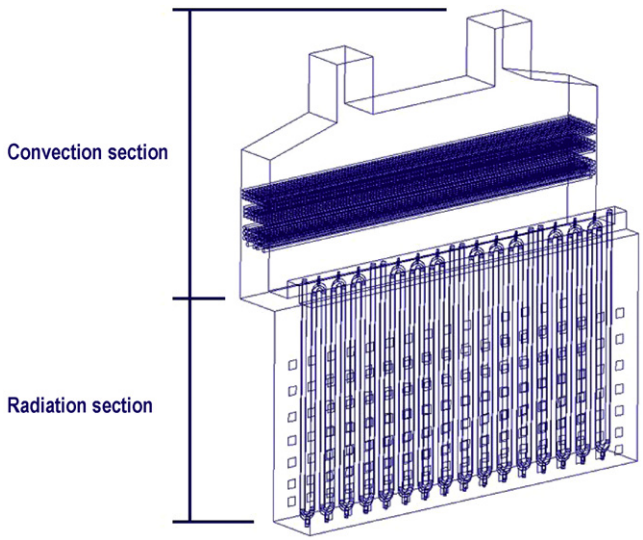

Fig. 1. Steam-cracking furnace with indication of the radiation and convection section.

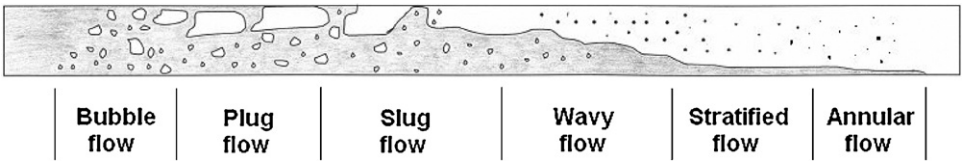

Fig. 2. Flow regimes during evaporation in a horizontal tube (after Thome, 2004).

two-phase vapor–liquid flow regime is also affected by interfacial tension forces, wetting characteristics of the liquid on the tube wall and momentum exchange between both phases. The prediction of the phase distribution in the tube is thus very difficult (Ghajar & Tang, 2007; Ghorai & Nigam, 2006; Kim & Ghajar, 2002).

The flow regimes encountered during the evaporation of a liquid flowing through a horizontal tube are shown in Fig. 2. The presented flow regimes are obtained when imposing a uniform, low heat flux on the tube wall. In first instance, the subcooled liquid, entering the horizontal tube, is heated. When the liquid temperature exceeds the saturation temperature near the tube wall, small bubbles develop and the bubble flow regime is observed. These bubbles coalesce and form larger bubbles, flowing along the top of the tube due to gravity effects. Vapor plugs and slugs are formed when the amount of vapor further increases: the plug and slug flow regime are observed. Meanwhile, smaller bubbles rise from the bottom of the tube and coalesce with these vapor plugs and slugs. A further increase of the vapor amount results in wavy flow. Finally, the remaining small liquid fraction flows as a film along the tube wall and the annular flow regime is observed. The most dramatic boiling transition occurs at the Critical Heat Flux (Celata, Mishima, & Zummo, 2001; Collier, 1981; Dhir, 1998). At this point, the liquid film at the wall dries out: this phenomenon is called Dryout (Chen & Costigan, 1993). The absence of a liquid film on the wall causes a sudden decrease of the heat transfer efficiency resulting in local overheating of the tube wall. In this so-called spray flow regime, small liquid droplets are dispersed in the vapor phase.

Remark that the sequence of the above-described flow regimes can differ, as they depend on several flow characteristics: liquid and vapor velocity, heat flux on the tube wall, viscosity and density of both phases. Consequently, not all flow regimes are necessarily encountered during the flow boiling process.

3. CFD modeling of flow boiling

The computation of boiling flows remains a challenge in computational fluid dynamics. These flows are characterized by the discontinuity of many of the flow variables across the phase interface. These discontinuities pose several computational difficulties requiring special treatment. In addition, the location of the phase interface is not known a priori and must be determined as a part of the solution procedure.

The simulation of boiling phenomena using CFD is possible by applying user-developed subroutines and linking them to the main hydrodynamic model equations. As a multiphase problem with mass exchange between the phases is considered, a model needs to be applied in the mass conservation equations of both phases. Analogously, the heat of evaporation must be accounted for in the energy equation. The complete CFD modeling approach for flow boiling is described next.

3.1. Multiphase flow model

Using the available CFD code, two-phase vapor–liquid flow regimes are calculated correctly (De Schepper, Heynderickx, & Marin, 2008). For these calculations, use is made of the Volume Of Fluid (VOF) model. In this multiphase flow model, an Eulerian–Eulerian approach is applied in which both fluids are assumed to behave as continuous media.

3.1.1. VOF model

In the VOF model, a single set of conservation equations, the well-known Navier–Stokes equations, is shared by the participating fluids. For a detailed analysis of the different terms in the conservation equations, reference is made to Anderson (1995) and Versteeg & Malalasekera (1995).

The liquid hydrocarbon feed is introduced in the heat exchanger tubes at a high velocity, causing a highly turbulent flow regime of the liquid phase. Furthermore, once the evaporation process starts, important velocity differences evolve between the two phases. A correct simulation of the turbulence effects is thus needed. Turbulent flows are characterized by fluctuating velocity fields. These fluctuations do not only mix the transported quantities such as momentum, energy and species concentrations, but cause fluctuations of these quantities as well. Since these fluctuations can be of small scale and high frequency, it is computationally too expensive to simulate them directly. To remove these small-scale fluctuations, the instantaneous conservation equations are averaged. This results in a modified set of equations, computationally less expensive to solve. Transformation of the instantaneous flow equations to conservation equations in the averaged variables, results in the Reynolds-averaged Navier–Stokes (RANS) equations, the so-called RANS equations. These equations can be found in Table 1. More detailed information concerning these equations may be found in Anderson (1995) and Versteeg & Malalasekera (1995).

It is straightforward to apply this set of conservation equations (Eqs. (1)–(3) in Table 1) to single-phase flows. For multiphase flow systems, however, the appropriate jump boundary conditions at the interfaces between the different phases are required. In particular, density, viscosity and other relevant physical properties change abruptly at the position of the interface.

The numerical solution, based on the finite volume approach (Versteeg & Malalasekera, 1995), of the set of Eqs. (1)–(3) in Table 1 for multiphase flows is extremely difficult and computationally intensive. The main difficulty arises from the interaction between the moving interface on one hand and the fixed Eulerian grid that is employed to solve the flow field on the other hand. Because the interface between the different phases does not necessarily remain stationary, imposing boundary conditions at an interface is a very complicated moving boundary problem. To avoid this problem, the VOF model directly determines the motion of all phases and deduces the motion of the interfaces indirectly from this result. Direct tracking of the motion and the deformation of the phase interfaces is thus avoided. All the interfacial forces, therefore, have to be replaced by smoothly varying volumetric forces. The corresponding methods, which describe and track the time-dependent behavior of the interface itself, are called front tracking methods (Zaleski, 2005).

Motion of the different phases is tracked by solving a continuity equation for the volume fraction of each phase. Thus, when a control volume is not entirely occupied by one phase, mixture properties are used while solving Eqs. (1)–(3) in Table 1. This approach

Table 1
Governing equations

Reynolds-averaged Navier–Stokes equations

$$\frac{\partial}{\partial t}(\rho)+\sum_{j=1}^{3}\frac{\partial}{\partial x_i}(\rho\bar{u}_i)=S_{\mathrm{M}} \tag{1}$$

$$\frac{\partial}{\partial t}(\rho\bar{u}_i)+\sum_{j=1}^{3}\frac{\partial}{\partial x_j}\cdot(\rho\bar{u}_i\bar{u}_j)=-\frac{\partial p}{\partial x_i}+\sum_{j=1}^{3}\frac{\partial}{\partial x_j}\left[\mu\left(\frac{\partial\bar{u}_i}{\partial x_j}+\frac{\partial\bar{u}_j}{\partial x_i}-\frac{2}{3}\delta_{ij}\sum_{l=1}^{3}\frac{\partial\bar{u}_l}{\partial x_l}\right)\right]+\sum_{j=1}^{3}\frac{\partial}{\partial x_j}(-\rho\overline{u_i'u_j'})+S_{\mathrm{F},i} \tag{2}$$

$$\frac{\partial}{\partial t}(\rho E)+\sum_{j=1}^{3}\frac{\partial}{\partial x_j}(\rho E\bar{u}_j)=\sum_{i=1}^{3}\sum_{j=1}^{3}\left(\frac{\partial}{\partial x_j}(\tau_{ij}-\rho\overline{u_i'u_j'})\bar{u}_i\right)-\sum_{j=1}^{3}\frac{\partial}{\partial x_j}q_j+S_{\mathrm{E}} \tag{3}$$

Reynolds stresses

$$-\rho\overline{u_i'u_j'}=\mu_{\mathrm{turb}}\left(\frac{\partial\bar{u}_i}{\partial x_j}+\frac{\partial\bar{u}_j}{\partial x_i}\right)-\frac{2}{3}\left(\rho k+\mu_{\mathrm{turb}}\sum_{l=1}^{3}\frac{\partial\bar{u}_l}{\partial x_l}\right)\delta_{ij} \tag{4}$$

Standard k–ε model

$$\frac{\partial}{\partial t}(\rho k)+\sum_{j=1}^{3}\frac{\partial}{\partial x_j}(\rho k\bar{u}_j)=\sum_{j=1}^{3}\frac{\partial}{\partial x_j}\left[\left(\mu+\frac{\mu_{\mathrm{turb}}}{\sigma_k}\right)\frac{\partial k}{\partial x_j}\right]+\bar{P}_k-\rho\varepsilon \tag{5}$$

$$\frac{\partial}{\partial t}(\rho\varepsilon)+\sum_{j=1}^{3}\frac{\partial}{\partial x_j}(\rho\varepsilon\bar{u}_j)=\sum_{j=1}^{3}\frac{\partial}{\partial x_j}\left[\left(\mu+\frac{\mu_{\mathrm{turb}}}{\sigma_\varepsilon}\right)\frac{\partial\varepsilon}{\partial x_j}\right]+C_{1\varepsilon}\frac{\varepsilon}{k}\bar{P}_k-C_{2\varepsilon}\rho\frac{\varepsilon^2}{k} \tag{6}$$

$$\bar{P}_k=\sum_{i=1}^{3}\sum_{j=1}^{3}\left[\left(\mu_{\mathrm{turb}}\left(\frac{\partial\bar{u}_i}{\partial x_j}+\frac{\partial\bar{u}_j}{\partial x_i}-\delta_{ij}\sum_{l=1}^{3}\frac{2}{3}\frac{\partial\bar{u}_l}{\partial x_l}\right)-\frac{2}{3}\rho k\delta_{ij}\right)\frac{\partial\bar{u}_j}{\partial x_i}\right] \tag{7}$$

$$\mu_{\mathrm{turb}}=\rho C_\mu\frac{k^2}{\varepsilon} \tag{8}$$

avoids abrupt changes in properties across very thin interfaces. The properties appearing in Eqs. (1)–(3) in Table 1 are converted to mixture properties based on the volume fraction of the different phases (Ranade, 2002):

$$\rho=\sum\alpha_k\rho_k \tag{9}$$

$$\mu=\sum\alpha_k\mu_k \tag{10}$$

However, in case of heat capacity, which has units of J/(kg K), a mass and not volume weighted interpolation is used in every computational cell (Ranade, 2002):

$$C_p=\frac{\sum\alpha_k\rho_k C_{p,k}}{\sum\alpha_k\rho_k} \tag{11}$$

For each additional phase added to the multiphase system, the volume fraction of that phase in the computational cell is introduced as an additional variable. In each computational cell, the volume fractions of all phases sum up to unity. All control volumes must be filled with either a single fluid phase or a combination of phases. The VOF model does not allow for void regions where none of the phases is present. The values of all variables and properties are calculated as volume-averaged values, as seen in Eqs. (9) and (10). They can only be determined when the volume fraction of each of the phases is known at a given location.

As mentioned before, a single set of conservation equations is solved throughout the computational domain. The properties appearing in these equations are determined by the presence of the phases in each computational cell. For example, the momentum equation (Eq. (2) in Table 1) depends on the volume fractions of all phases through the properties density and viscosity. If only liquid is present in a given computational cell, the physical properties of only the liquid phase will be used and thus the velocity of the liquid phase is obtained. The same holds for computational cells where only vapor phase is present. However, if both phases are present in a computational cell, the mixture properties will be calculated, making use of Eqs. (9) and (10). Solution of the momentum equation in that given computational cell results in the velocity shared by the phases. By application of the PLIC interface reconstruction method (see Section 3.1.2), the velocities of the phases present close to the interface are determined (Zaleski, 2003). Making use of an advection algorithm, implemented in the PLIC method, the advecting amount of fluid through each cell face is calculated. Knowing the face fluxes and the normal and tangential velocity distribution in the grid cell, the velocities of both phases are calculated. One limitation of this shared-fields approximation is that in situations where large velocity differences exist between the phases, the calculation of the velocities of the phases near the interface may be less accurate.

Also one energy equation is solved throughout the computational domain. The density and thermal conductivity are calculated as in Eqs. (9) and (10). Near the interface, solution of the energy equation results in a temperature field shared by the phases. The VOF model treats the total energy and temperature as mass-averaged variables:

$$E=\frac{\sum_{k=1}^{n}\alpha_k\rho_k E_k}{\sum_{k=1}^{n}\alpha_k\rho_k} \tag{12}$$

The total energy for each phase E_k is based on the specific heat of that phase and the shared temperature. From this shared temperature, the temperature of the phases in a grid cell is to be

determined. In this work, the interfacial temperature is assumed to be the saturation temperature. This temperature condition is a common approximation for which justification may be found in Son & Dhir (1998). Given the orientation of the planar surface representing the interface in a grid cell and given the data concerning the location of this interface, this temperature condition is applied to the point located at the center of the piecewise linear segment (Welch & Wilson, 2000). It is then straightforward to calculate the liquid side temperature gradients as well as the vapor side temperature gradients, knowing the temperatures of the phases in the neighboring grid cells. As for the velocity field, the accuracy of the temperature near the interface is limited in situations where large temperature differences exist between the phases.

The volume fraction of each phase is calculated by tracking the interface between the different phases throughout the complete solution domain. Tracking of the interfaces between N different phases present in the system is accomplished by solving the continuity equations for the phase volume fraction of $N-1$ phases. For the kth phase, this equation has the following form:

$$\frac{\partial \alpha_k}{\partial t} + \sum_{j=1}^{3} \frac{\partial}{\partial x_j}(\alpha_k \bar{u}_j) = S_{\alpha_k} \tag{13}$$

For more information concerning the different terms in this equation, reference is made to Ranade (2002) and De Schepper, Heynderickx, & Marin (2008). By solving continuity equation (13) for $N-1$ phases, the value of the volume fraction of all phases is determined throughout the complete solution domain. It must, however, be noted that the phase volume fraction values do not uniquely identify the interface. Different interface configurations result in identical volume fractions for the N phases. Consequently, several specialized techniques are developed to track the geometry of the interface accurately (Zaleski, 2005). The applied technique in this work is described in the next paragraph. For more information concerning other interface reconstruction techniques, reference is made to De Schepper, Heynderickx, & Marin (2008).

3.1.2. Interpolation near the interface

In general, a VOF algorithm (Zaleski, 2005) solves the problem of updating the phase volume fraction field in the fixed grid, based on the velocity field and the phase volume fraction field as determined in the previous time step. In a two-dimensional problem, the interface is considered to be a continuous, piecewise smooth line. The problem is then reduced to the reconstruction of an approximation of the interface in each cell, based on the volume fraction of each phase in that cell and in the neighboring cells.

The most accurate VOF techniques attempt to fit the interface through piecewise linear segments. These techniques are known as the Piecewise Linear Interface Calculation (PLIC) algorithms (Li, 1995). In the PLIC approach, an interface within a computational cell of the fixed grid in a two-dimensional problem is approximated by a straight line segment with a slope determined from the interface normal. The line segment cuts the computational cell such that the volumes of the phases in the cell correspond with the values of the phase volume fractions in that cell. The resulting fluid polygon is then used to determine the possible fluxes of the different phases through a cell face. For more information concerning the procedure of a VOF/PLIC algorithm, reference is made to De Schepper, Heynderickx, & Marin (2008), Puckett (1991), and Puckett, Almgren, Bell, Marcus, & Rider (1997).

During all simulations in the presented work, a PLIC reconstruction approach has been used. Considering the available techniques, it is the most accurate one and it is applicable for general unstructured meshes as the one used here. In this work, only two phases are considered, which implies that only one equation (13) needs to be solved and only interface needs to be determined.

3.1.3. Turbulence model

The RANS equations describe the transport of the averaged flow quantities, with the whole range of the turbulence scales being modeled. Due to the averaging, these equations contain additional unknown variables. These unknown variables, called Reynolds stresses, are modeled in terms of known quantities, making use of so-called "closure models" such as turbulence models (Versteeg & Malalasekera, 1995). A number of turbulence models, following the RANS-based modeling approach have been developed: the Spalart–Allmaras model (Spalart & Allmaras, 1992), the k–ε model (Launder & Spalding, 1972) and variants, the k–ω model (Wilcox, 1998) and variants and the Reynolds Stress model (Gibson & Launder, 1978). Since the standard k–ε model has been used for the simulations presented in this work, this model will be further explained.

By application of the Boussinesq hypothesis (Versteeg & Malalasekera, 1995), the Reynolds stresses are related to the mean velocity gradients. The expression for the calculation of these Reynolds stresses corresponds with Eq. (4) in Table 1. To be able to solve this equation, an expression for the turbulent viscosity is needed. Using the standard k–ε model, the calculation of the turbulent viscosity μ_{turb} is computationally non-expensive. In a first step, two additional transport equations for the turbulent kinetic energy k and the viscous dissipation of the turbulent kinetic energy ε are solved, which correspond with Eqs. (5) and (6) in Table 1. Finally, the turbulent viscosity is calculated as a function of k and ε (Eq. (8) in Table 1).

3.2. Mass and energy transfer during the evaporation process

The CFD software package Fluent 6.3 (Fluent Inc., 2006), used in this work, does not dispose over a model that is able to simulate the evaporation process itself in a correct way. In order to overcome this problem, an in-house developed code will be used to complete the existing CFD code. This in-house developed code is especially required to calculate the mass and energy transfer between both phases during the evaporation process. This transfer is determined by the source terms S_{M} and S_{E} in Eqs. (1) and (3) in Table 1, respectively. In order to construct an appropriate mass transfer code, applicable mass transfer expressions need to be found in literature or derived in this work. Several expressions have been found in literature and will be presented next.

Many expressions describing the mass transfer during evaporation are based on the kinetic gas theory. A well-known equation for the net mass flux over the vapor–liquid interphase during the evaporation process is the Hertz–Knudsen equation (Knudsen, 1934):

$$J' = \alpha_{\text{c}} \frac{\sqrt{M}}{\sqrt{2\pi R}} \left(\frac{p}{\sqrt{T_{\text{v}}}} - \frac{p_{\text{sat}}(T_{\text{l}})}{\sqrt{T_{\text{l}}}} \right) \tag{14}$$

In this equation, α_{c} is the accommodation coefficient. In case of condensation, α_{c} is defined as the ratio of the experimentally observed condensation velocity and the maximal theoretical condensation velocity. On the other hand, in case of evaporation, this parameter is defined as the ratio of the experimentally observed evaporation velocity and the maximal theoretical evaporation velocity. The accommodation coefficient may be expressed as a function of the condensation coefficient σ_{c} for a condensation process or the evaporation coefficient σ_{e} for an evaporation process (Knudsen, 1934):

Condensation:

$$\alpha_c = \frac{2\sigma_c}{2-\sigma_c} \tag{15}$$

Evaporation:

$$\alpha_c = \frac{2\sigma_e}{2-\sigma_e} \tag{16}$$

The condensation and evaporation coefficient will be discussed later.

The Clausius–Clapeyron equation (Lide, 1998) relates the pressure with the temperature under saturation conditions:

$$\frac{dp}{dT} = \frac{\Delta H}{T(1/\rho_v - 1/\rho_l)} \tag{17}$$

By approximation, this equation can yield the following formula as long as the pressure and temperature are close to the saturation conditions:

$$p - p_{sat} = -\frac{\Delta H}{T(1/\rho_v - 1/\rho_l)}(T - T_{sat}) \tag{18}$$

Substitution of Eq. (18) in the Hertz–Knudsen equation (14) results in:

$$J' = \alpha_c \frac{\sqrt{M}}{\sqrt{2\pi R T_{sat}}} \frac{\Delta H}{(1/\rho_v - 1/\rho_l)} \frac{T_{sat} - T}{T_{sat}} \tag{19}$$

As mentioned before, the mass transfer due to phase change is introduced in the mass conservation equation (Eq. (1) in Table 1) via the source term. In order to correctly add this source term, the mass flux should be expressed in kg/m^3 s. Multiplication of Eq. (19) with the volumetric interfacial surface area a_i converts the mass flux into the correct units. Consequently, the expression for the mass flux over the liquid–vapor interface is given by

$$J = a_i \alpha_c \frac{\sqrt{M}}{\sqrt{2\pi R T_{sat}}} \frac{\Delta H}{(1/\rho_v - 1/\rho_l)} \frac{T_{sat} - T}{T_{sat}} \tag{20}$$

The volumetric interfacial surface area is related to the mean Sauter diameter D_{Sm} (Crowe, Sommerfeld, & Tsuji, 1998) and the volume fraction of the phase under consideration:

$$a_i = \frac{6\alpha_k}{D_{Sm}} \tag{21}$$

assuming spherical bubbles.

In order to implement Eq. (20) in a user-developed subroutine, an expression for the accommodation coefficient α_c and the volumetric interfacial surface area a_i are required.

Determination of the accommodation coefficient requires expressions for the condensation coefficient (condensation process) or the evaporation coefficient (evaporation process). The condensation coefficient of a vapor phase has been defined by Knudsen (1934) as the fraction of the number of vapor molecules impinging on a vapor–liquid interface that actually condense. The same definition may be given for the evaporation coefficient. Research has been carried out to determine the condensation and evaporation coefficient. If the condensation (evaporation) coefficient equals unity, the condensation (evaporation) process is complete, that is, every vapor (liquid) molecule, reaching the vapor–liquid interface, condenses (evaporates). If on the contrary the condensation (evaporation) coefficient is smaller than unity, an incomplete condensation (evaporation) is observed, where some of the vapor (liquid) molecules bounce back on the vapor–liquid interface into the vapor (liquid) phase. When the interface is at equilibrium, no net condensation or evaporation is observed and the evaporation coefficient equals the condensation coefficient. In many publications, the evaporation coefficient is not distinguished from the condensation coefficient, both terms are rather used as synonyms (Marek & Straub, 2001).

Making use of an improved molecular gas dynamics method, the condensation coefficient of methanol was determined as having a value between 0.8 and 0.9 (Mikami, Kobayashi, Ota, & Fujikawa, 2006). Analogously, the condensation coefficient of hexane and hexadecane has been estimated as respectively 0.9 and approximately 1.0 (Xia & Landman, 1994). The boiling points for hexane and hexadecane are respectively 371 K and 560 K. These values correspond with the range of boiling temperatures of the hydrocarbon feedstock that will be evaporated in this work. Based on the above considerations, the condensation and evaporation coefficient is given a value of 1.0 in the user-developed subroutine. Taking into account Eqs. (15) and (16), the corresponding accommodation coefficients have a value of 2.0.

To determine the volumetric interfacial surface area a_i, two methods are available. In the first method, correlations for the volumetric interfacial surface area are developed, making use of information on the two-phase vapor–liquid flow regime. In the second method, it is assumed that the volumetric interfacial surface area changes dynamically, which implies that a transport equation for the volumetric interfacial surface area is solved. Both methods will be discussed next.

In the first approach, the influence of flow regimes on different interface structures is analyzed. Based on the results, expressions have been developed for the volumetric interfacial surface area, mostly valid for the bubble flow regime. These expressions are semi-empirical correlations. Examples of typical expressions for the volumetric interfacial surface area for non-boiling bubble flow regimes can be found in Hibiki & Ishii (2000, 2001, 2002). Unlike for non-boiling bubble flow, it seems difficult to derive expressions in which the volumetric interfacial surface area explicitly depends on flow parameters typical for flow boiling such as the void fraction (Hetsroni, 2003). The latter expressions should be applicable for all developing flow regimes, observed during the flow-boiling process. Recently, an expression for the volumetric interfacial surface area valid for boiling bubbly flows has been developed by Hibiki, Lee, Lee, & Ishii (2006):

$$a_i \mathrm{Lo} = 3.6844 N_{\mathrm{Lo}}^{0.335} \varepsilon^{0.83} N_\rho^{-0.138} N_{Re_b}^{0.239} = 3.6844 \left(\frac{\mathrm{Lo}}{D_H}\right)^{0.335} \varepsilon^{0.83} \left(\frac{\rho_l}{\rho_v}\right)^{-0.138} \left(\frac{\varepsilon^{1/3}\mathrm{Lo}^{4/3}}{\upsilon_l}\right)^{0.239} \tag{22}$$

Note that the volumetric interfacial surface area is affected by the phase change, expressed by the void fraction ε. The Laplace length Lo (Hibiki, Lee, Lee, & Ishii, 2006) is defined as:

$$\mathrm{Lo} = \sqrt{\frac{\sigma}{g\ \Delta\rho}} \tag{23}$$

The Laplace length Lo and the bubble Reynolds number N_{Re_b} are important parameters, because they govern the bubble coalescence and break-up during the boiling process. The latter are necessary to describe the interaction of the generated bubbles in the boiling process. The pressure dependence of the volumetric interfacial surface area is taken into account by means of the density ratio N_ρ, which is often used as a scaling parameter for two-phase flow systems.

Attempts have been made to implement this expression in the user-developed subroutine. However, no reasonable results have been obtained. Since only liquid is fed at the inlet of the heat exchanger tube, the void fraction has an initial value of 0. Consequently, the initial value of the volumetric interfacial surface area and thus mass transfer expression is 0. This implies that no evaporation of liquid is observed even when the liquid temperature reaches the saturation temperature. Eq. (22) can thus only

be applied when already some vapor is present in the tube. It is thus clear that this expression for the volumetric interfacial surface area is not appropriate for implementation in the user-developed subroutine. Furthermore, the expression remains limited to bubbly flow regimes, while different flow regimes will be seen to develop during the evaporation process.

In the second method, the dynamical changes of the interfacial structure due to the phase change are taken into account. This implies that a transport equation for the volumetric interfacial surface area is solved together with the conservation equations for mass, momentum and energy. It is clear that the latter requires a huge computational effort and hence, it is not possible to use this method in the user-defined subroutine. More information concerning the development of a transport equation for the volumetric interfacial surface area can be found in Ishii, Kim, & Uhle (2002).

Therefore, another approach is taken. Under the assumption that the condensation and evaporation coefficient of the hydrocarbon feedstock has a value of 1.0 and using Eq. (21) for the volumetric interfacial surface area, the expression for the mass flux over the liquid–vapor interface (Eq. (20)) can be written as:

$$J = \frac{6}{D_{Sm}}\alpha\frac{\sqrt{M}}{\sqrt{2\pi R T_{sat}}}\frac{\Delta H}{(1/\rho_v - 1/\rho_l)}\frac{T_{sat}-T}{T_{sat}} \tag{24}$$

Based on the above equation and by introducing two parameters β_1 and β_2, the following expressions to calculate the mass transfer from liquid to vapor (evaporation) and from vapor to liquid (condensation) can be written:

$$J_{lv} = \beta_1\alpha_l\rho_l\frac{T_{sat}-T}{T_{sat}} \tag{25}$$

$$J_{vl} = \beta_2\alpha_v\rho_v\frac{T_{sat}-T}{T_{sat}} \tag{26}$$

The so-called mass transfer time relaxation parameters β_1 and β_2 determine the rate of evaporation and condensation:

$$\beta_1 = \frac{6}{D_{Sm}}\frac{\sqrt{M}}{\sqrt{2\pi R T_{sat}}}\frac{\rho_v\ \Delta H}{\rho_l - \rho_v} \tag{27}$$

$$\beta_2 = \frac{6}{D_{Sm}}\frac{\sqrt{M}}{\sqrt{2\pi R T_{sat}}}\frac{\rho_l\ \Delta H}{\rho_l - \rho_v} \tag{28}$$

According to the work of Lee (1980) and Wu, Peng, Ye, & Eric Gong (2007), the value of these parameters may be set equal to 0.1. It was shown that excessively large values of β_1 and β_2 cause a numerical convergence problem, while too small values lead to a significant deviation between the interfacial temperature and the saturation temperature (Lee, 1980; Yang, Peng, & Ye, 2007). By introducing the value 0.1 in Eqs. (25) and (26), the mass flux over the liquid–vapor interface, respectively, for the evaporation and condensation process can be calculated as:

$$J_{lv} = 0.1\alpha_l\rho_l\frac{T_{sat}-T}{T_{sat}} \tag{29}$$

$$J_{vl} = 0.1\alpha_v\rho_v\frac{T_{sat}-T}{T_{sat}} \tag{30}$$

The latter expressions have been implemented in the user-developed subroutine, which is linked to the main governing equations of the multiphase flow model (Table 1). The general construction of the user-developed subroutine can be found in Table 2. The expressions in this table are introduced as the interphase mass source term S_M in Eq. (1). As mentioned before, in the VOF model, one mass conservation equation is solved for the total computational domain. Again, the VOF model determines the fraction of vapor and liquid in a grid cell. Thus, two expressions describing the mass transfer during the evaporation process are required: one for the liquid phase (Eq. (31) in Table 2) and one for the vapor phase (Eq. (32) in Table 2). This can be explained by the fact that the continuous evaporation of liquid results in a liquid volume fraction decrease and a vapor volume fraction increase. Consequently, the decreasing amount of liquid and increasing amount of vapor should be calculated in the mass conservation equation. The user-developed subroutine is constructed in such a way that the correct expression is used as source term depending on the phase under consideration.

Table 2
Construction of the user-developed subroutine

Evaporation $T_l > T_{sat}$		
Liquid phase	$S_M = -0.1\alpha_l\rho_l\left\lvert\frac{T_l - T_{sat}}{T_{sat}}\right\rvert$	(31)
Vapor phase	$S_M = 0.1\alpha_l\rho_l\left\lvert\frac{T_l - T_{sat}}{T_{sat}}\right\rvert$	(32)
Condensation $T_v < T_{sat}$		
Liquid phase	$S_M = 0.1\alpha_v\rho_v\left\lvert\frac{T_v - T_{sat}}{T_{sat}}\right\rvert$	(33)
Vapor phase	$S_M = -0.1\alpha_v\rho_v\left\lvert\frac{T_v - T_{sat}}{T_{sat}}\right\rvert$	(34)
Energy		
Evaporation	$S_E = -0.1\alpha_l\rho_l\left\lvert\frac{T_l - T_{sat}}{T_{sat}}\right\rvert\Delta H$	(35)
Condensation	$S_E = 0.1\alpha_v\rho_v\left\lvert\frac{T_v - T_{sat}}{T_{sat}}\right\rvert\Delta H$	(36)

In Table 2, it can also be seen that the user-developed subroutine is constructed in such a way that both evaporation and condensation processes can be calculated. Consequently, if the vapor phase reaches a zone in the geometry where the temperature is lower than the saturation temperature, the condensation of vapor can also be calculated. Depending on the process under consideration, the correct interphase mass source term is calculated for both the liquid (Eq. (33) in Table 2) and vapor phase (Eq. (34) in Table 2).

As mentioned before, a source term S_E representing the evaporation or condensation heat should be added to the energy equation. In the VOF model, only one energy equation is solved for both phases. Consequently, only one expression is required for the calculation of the heat transfer during the evaporation or condensation process. The heat transfer corresponding with the evaporation or condensation process is determined by multiplying the calculated mass transfer with the latent heat. The correct expressions for the calculation of this heat transfer, implemented in the user-developed subroutine, can be found in Table 2.

Finally, no momentum exchange between the phases is assumed. Consequently, the source term $S_{F,i}$ in the momentum equation is 0.

4. Simulations

4.1. Tube geometry and operating conditions

The flow boiling of a hydrocarbon feedstock in the convection section heat exchanger of a steam cracker is simulated. One tube in this heat exchanger is made out of four horizontal passes, each with a length of 11.3 m and a diameter of 0.0525 m. These four passes are connected by two vertical bends and one horizontal bend. The horizontal bend is located between the second and third pass. The complete 3D-computational domain is divided into 1,993,648 hex-

Table 3
Physical properties of gasoil–liquid and gasoil–vapor

	Gasoil–liquid	Gasoil–vapor
Density (kg/m^3)	649	9.6
Heat capacity (kJ/kg K)	2.399	2.069
Viscosity (Pa s)	0.00332	7×10^{-6}

ahedral cells. Near the tube wall, three layers of cells are positioned to assure a correct simulation of the phenomena taking place near the wall.

A typical hydrocarbon feedstock contains a range of hydrocarbons with varying physical properties. To avoid having to take this problem into account as well, a reference material is used. This material is defined as gasoil–liquid and gasoil–vapor. To limit the calculation time, the physical properties of the reference material are assumed to be constant, that is temperature-independent. These constant physical properties of the gasoil–liquid and the gasoil–vapor represent averaged values of a typical hydrocarbon feedstock and can be found in Table 3.

Furthermore, in the user-developed subroutine for the calculation of the mass and energy transfer during the evaporation process, the boiling temperature of the gasoil–liquid is defined as 380 K. The latent heat is given a value of 210.68 kJ/kg.

In order to simulate the heating and evaporation of the hydrocarbon feedstock in the convection section heat exchanger tubes, a realistic heat flux should be defined at the wall boundaries. These heat fluxes are to be determined based on CFD calculations of the flue gas flow and temperature field over the heat exchanger tubes in the convection section box. In this work however, a constant heat flux is imposed as boundary condition on the tube wall of each of the four straight passes. The values of these heat fluxes can be found in Table 4. The bends, which connect the four straight passes, are located outside the convection section box. Therefore, a zero heat flux is defined as boundary condition on these bends, assuming a perfect insulation.

In the simulation, a no-slip condition for both phases is imposed at the tube walls. The influence of the gravitational force on the flow has been taken into account. At the inlet of the heat exchanger tube, uniform profiles for all the variables have been imposed. A pressure outlet boundary is imposed to avoid problems with backflow at the outlet of the tube.

4.2. Solution strategy and convergence criterion

Prior to the transient two-phase flow simulation, a steady-state simulation is carried out to determine the flow and temperature field of the reference material gasoil–liquid. Gasoil–liquid with a temperature of 350 K is fed at the tube inlet with a mass flow rate of 0.729 kg/s. The fluid pressure at the tube inlet is set to 380 kPa. In this simulation, only flow and heating of the gasoil–liquid throughout the heat exchanger are calculated. The fully converged steady-state flow and temperature field of gasoil–liquid is used as the starting point for the two-phase flow simulation. The VOF model and the user-developed subroutines are enabled and the transient simulation is started, the results of which will be discussed in the next paragraph.

Table 4
Heat flux values imposed on the walls of the horizontal tubes

	Heat flux (kW/m^2)
Tube 1	44.2
Tube 2	33.5
Tube 3	33.5
Tube 4	30.6

Because of the dynamic behavior of the two-phase flow and the flow boiling process, a transient simulation with a time step of 0.001 s is carried out. The calculations are performed by combination of the PISO algorithm (Issa, 1986) for pressure–velocity coupling and a second-order upwind calculation scheme (Versteeg & Malalasekera, 1995) for the determination of momentum, volume fraction and energy. The convergence is based on the residual value of the calculated variables, namely mass, velocity components, volume fraction and temperature. In the presented calculations, the numerical computation is considered to be converged when the scaled residuals of the variables mass, velocity components and volume fraction have lowered by four orders of magnitude and when the residuals of the temperature variable have lowered by six orders of magnitude.

For the simulation of the transient flow boiling process, use is made of a personal computer with dual 3.0 GHz processor, 4 GB RAM and a Linux operating system. A calculation time of 3 months was necessary to obtain the presented results.

When the transient simulation is started, 'fresh' gasoil–liquid with an inlet temperature of 350 K enters the heat exchanger tube. While the liquid flows through the tube, it is heated first. Once the boiling temperature (380 K) is reached, evaporation starts. The evolving vapor phase has a higher velocity than the liquid phase and thus influences the initial flow and temperature field for the gasoil–liquid obtained from the steady-state simulation. However, a complete analysis of the flow boiling process in the heat exchanger tube can only be made when the liquid phase fed at time step zero of the transient simulation reaches the outlet of the tube. After simulating 14.67 s of real time (residence time), a complete simulation of the flow boiling process is obtained.

4.3. Simulation results

The simulation results of the evaporation process of gasoil–liquid in a tube of a convection section heat exchanger are discussed next. The simulated time is 14.67 s.

Fig. 3 represents the volume fraction field of the gasoil–liquid in the geometry. A red color stands for the presence of only gasoil–liquid (liquid volume fraction = 1), while a blue color implies the presence of only gasoil–vapor (liquid volume fraction = 0). In Fig. 3, focus is made on areas of the first, second and third horizontal passes where a specific two-phase flow regime can be clearly observed.

The liquid phase entering the heat exchanger tube is heated in the first part of the geometry. As such, in the first 6 m of the tube, only liquid is observed. Next, the liquid phase starts to evaporate at positions where the boiling temperature is reached. At those positions, bubbles start to form and accumulate at the top of the tube due to the gravity effect. Following this bubble formation, a succession of different horizontal two-phase flow regimes is seen to develop. Due to the increasing amount of vapor, which has a higher velocity than the liquid phase, the two-phase flow regime becomes more chaotic. A growing amount of bubbles accumulate at the top of the tube and plug flow is observed. As the liquid flows further through the tube, the amount of vapor phase and thus the vapor velocity increases. Liquid slugs, containing small vapor bubbles can be seen. The slug flow regime is even more chaotic as compared to the plug flow regime and the interface between the liquid slugs and the elongated gas bubbles is less sharp. This slug flow regime is observed near the end of the second horizontal pass and in the third horizontal pass. In the last horizontal pass, a combination of wavy and stratified flow is observed. From the calculation it is concluded that vapor phase is generated in all four tube passes. Due to the presence of the bends, the vapor phase is redistributed as a consequence of geometrical changes of

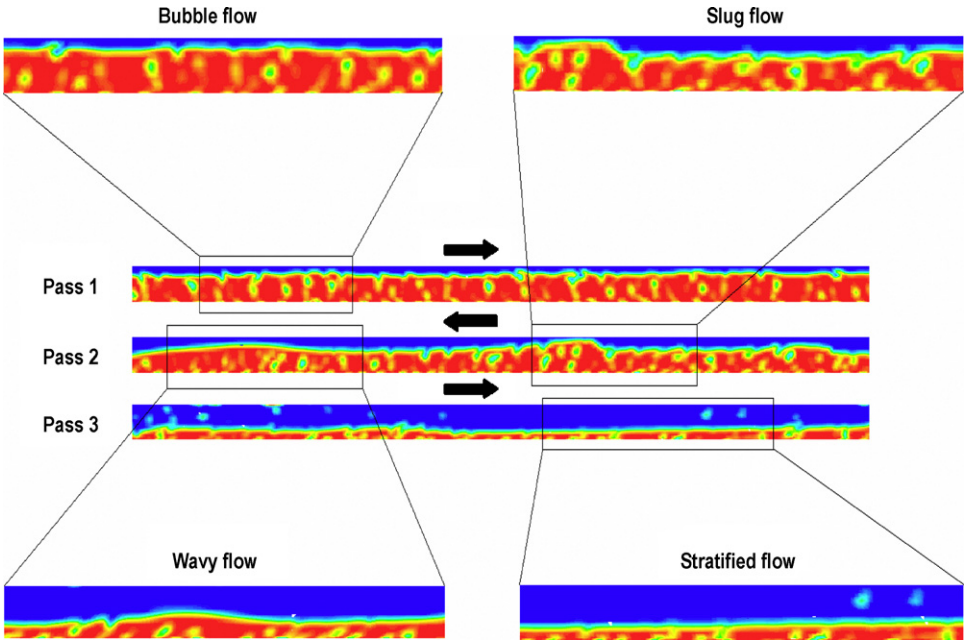

Fig. 3. Volume fraction field of gasoil–liquid flowing in a convection section tube of a steam cracker (red = gasoil–liquid, blue = gasoil–vapor).

the tube. In these adiabatic bends, re-condensation of the vapor is possible.

The temperature field of both phases in the neighborhood of the first vertical bend is presented in Fig. 4b. As explained before, the liquid phase is heated in the first 6 m of the tube. When the boiling temperature of 380 K is reached, evaporation of the liquid phase takes place and a vapor phase is formed. The vapor phase accumulates above the liquid phase. It is observed in Fig. 4b that the temperature of this accumulated vapor phase increases due to overheating. After the first vertical bend, a high temperature increase is observed. However, due to an alternating flow of liquid and vapor phase in the top of the second tube pass, which is typical for the slug flow regime, only a small increase in wall temperature is calculated. At given positions in the tube, a local temperature increase is calculated. This indicates that vapor is present at these locations. Analogously, the lower temperature zones indicate the presence of a liquid slug. Starting from the middle of the third tube pass, the temperature profile is very uniform, due to the high amount of vapor present. It is calculated that the temperature at the bottom of the third and fourth tube pass is much lower than at the top of the tube pass, due to the presence of the liquid phase remaining there. Nevertheless, the temperature of the liquid flowing over the bottom of the last two tube passes is still higher than the saturation temperature. This is caused by the high temperature of the small vapor bubbles formed at the lower tube wall and rising through the liquid phase. Remark that the calculated temperature fields represent an ideal situation, where a uniform heat flux is imposed on each of the tube walls, see Table 4. A more accurate simulation of the flow boiling process in the convection section tubes requires a coupled simulation of the flue gas side and process gas side in the steam cracker convection section. A coupled simulation results in heat flux profiles to and wall temperature profiles on the convection section tubes.

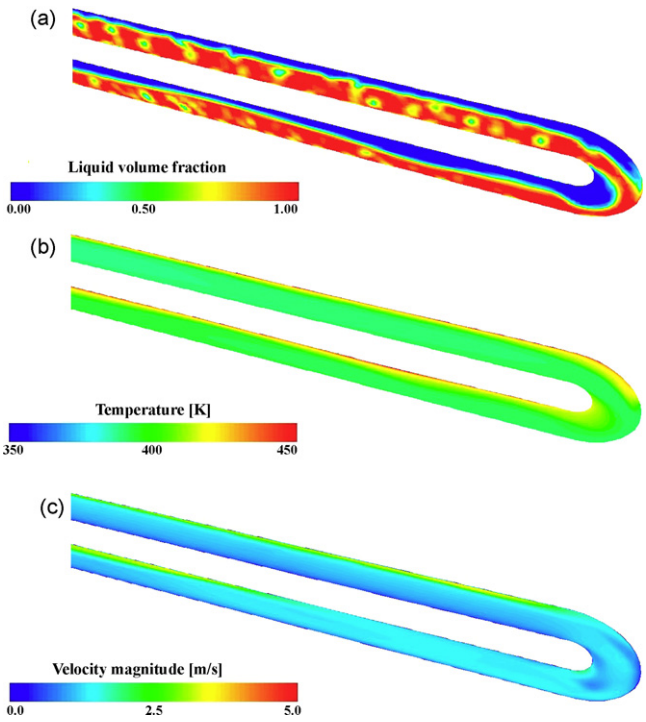

Fig. 4. Flow boiling process of gasoil–liquid in a heat exchanger tube: (a) volume fraction field of the liquid phase, (b) temperature field and (c) velocity magnitude field.

Fig. 4c represents the velocity magnitude field of both phases in the neighborhood of the first vertical bend. In this figure, it can be clearly seen that both phases have a different velocity. Moreover, the vapor phase has a much higher velocity than the liquid phase. This difference in velocity causes the development of the slug and wavy two-phase flow regimes.

A total pressure drop of 42 kPa is calculated over the whole tube length. However, the pressure drop per tube pass changes. A pressure drop of about 2 kPa is calculated over the first tube pass, while this pressure drop increases to about 7 and 8 kPa, respectively, over the second and third pass. The rising pressure drop can be explained by the two-phase flow regime with rising vapor fraction in the tube passes. Due to the more turbulent and chaotic character of the slug flow regime in tube pass three and four, a higher pressure drop is

calculated. In the last tube pass, an even higher pressure drop of about 15 kPa is calculated. This is explained by the high velocity of the vapor phase.

As can be concluded from the simulation results presented in the figures and the discussion made above, the succession of the observed horizontal two-phase flow regimes agrees well with the expected phenomena during flow boiling as found in literature (Thome, 2004). Furthermore, the phenomena, typical for each flow regime, can be distinguished on the figures.

Once again, a coupled simulation of the flue gas side and process gas side of the steam cracker convection section is required to validate the applied models. Simulation results can then indirectly be evaluated by comparing the calculated outlet temperatures for the flue gas and the process gas with the industrially measured values. At this moment, a first evaluation of the results can be made, based on the mass-weighted volume fraction of the phases. The mass-weighted volume fraction of the liquid phase at the outlet is 0.49. From industrial data, it is expected that 70% of the liquid is evaporated at the outlet of the feed preheat and evaporation heat exchanger in the convection. This corresponds with an outlet mass-weighted volume fraction of 0.3. The difference between the simulated and industrial value is most likely explained by the fact that a uniform heat flux is imposed on the tube walls, while a correct simulation requires a coupled simulation of flue gas side and all heat exchangers. Another possible explanation is the difference between the industrial hydrocarbon feed composition and the reference liquid used in this work. Furthermore, the physical properties of the gasoil–liquid and gasoil–vapor were assumed to be constant. Consequently, in order to obtain a more accurate simulation of the evaporation process in the feed preheat and evaporation heat exchanger in the steam cracker convection section, a more extended simulation should be carried out. A detailed heat flux profile from the flue gas to the tube walls should be imposed as thermal boundary condition. Furthermore, the variation of the physical properties of both phases with temperature should be taken into account. However, it is clear that this will require a higher computational effort.

5. Conclusions

The main purpose of the presented work is the development of a model that allows to perform 3D-simulations of the evaporation process of a hydrocarbon feedstock in a heat exchanger of the convection section of a steam cracker. The calculation of the evaporation process is one of the steps required to complete the research on convection section modeling.

The heating, evaporation and boiling phenomena occurring at conditions typical for the convection section of a steam cracker could be modeled adequately by implementing the appropriate source terms in the conservation equations. These source terms, describing the mass and heat transfer during the evaporation process, have been derived from the Hertz–Knudsen equation.

A simulation of the evaporation of a hydrocarbon feedstock in a tube of the convection section was performed based on a constant heat flux profile and constant hydrocarbon physical properties. The outlet conditions of the partially evaporated hydrocarbon feedstock are discussed.

In order to obtain an even more accurate simulation of the flow boiling process in the convection section heat exchanger, additional improvements are required. The variation of the physical properties of the liquid and vapor phase with temperature must be taken into account and a detailed heat flux profile should be imposed as thermal boundary condition on the tube walls. However, this will require an even more extensive computational effort.

References

Anderson, J. D. (1995). *Computational fluid dynamics: The basics with applications*. New York: McGraw-Hill.

Cai, H., Krzywicki, A., & Oballa, M. C. (2002). Coke formation in steam crackers for ethylene production. *Chemical Engineering and Processing*, *41*, 199.

Celata, G. P., Mishima, K., & Zummo, G. (2001). Critical heat flux prediction for saturated flow boiling of water in vertical tubes. *International Journal of Heat and Mass Transfer*, *44*, 4323.

Chen, J. C., & Costigan, G. (1993). Review of post-dryout heat transfer in dispersed two phase flow. *Multiphase Science and Technology*, *7*, 1.

Collier, J. G. (1981). *Convective boiling and condensation* (2nd ed.). New York: Mc Graw-Hill.

Crowe, C., Sommerfeld, M., & Tsuji, Y. (1998). *Multiphase flows with droplets and particles*. CRC Press.

De Schepper, S. C. K., Heynderickx, G. J., & Marin, G. B. (2008). CFD modeling of all gas–liquid and vapor–liquid flow regimes predicted by the Baker chart. *Chemical Engineering Journal*, *138*, 349.

Dhir, V. K. (1998). Boiling heat transfer. *Annual Review of Fluid Mechanics*, *30*, 365.

Fluent Inc. (2006). *Fluent 6.3 user's guide*. Lebanon/USA: Fluent Inc.

Ghajar, A. J., & Tang, C. C. (2007). Heat transfer measurements, flow pattern maps and flow visualization for non-boiling two-phase flow in horizontal and slightly inclined pipe. *Heat Transfer Engineering*, *28*, 525.

Ghorai, S., & Nigam, K. D. P. (2006). CFD modeling of flow profiles and interfacial phenomena in two-phase flow in pipes. *Chemical Engineering and Processing*, *45*, 55.

Gibson, M. M., & Launder, B. E. (1978). Ground effects on pressure fluctuations in the atmospheric boundary layer. *Journal of Fluid Mechanics*, *86*, 491.

Hetsroni, G. (2003). *Flow regimes, pressure drop and void fraction*. Lecture given at Short Course: Modeling and Computation of Multiphase Flows, Part 1: Bases. Hosted by the Swiss Federal Institute of Technology, Zurich, Switzerland.

Heynderickx, G. J., Oprins, A. J. M., Dick, E., & Marin, G. B. (2001). Three-dimensional flow patterns in cracking furnaces with long-flame burners. *AIChE Journal*, *47*, 388.

Hibiki, T., & Ishii, M. (2000). One-group interfacial area transport of bubbly flows in vertical round tubes. *International Journal of Heat and Mass Transfer*, *43*, 2711.

Hibiki, T., & Ishii, M. (2001). Interfacial area concentration in steady fully-developed bubbly flow. *International Journal of Heat and Mass Transfer*, *44*, 3443.

Hibiki, T., & Ishii, M. (2002). Interfacial area concentration of bubbly flow systems. *Chemical Engineering Science*, *57*, 3967.

Hibiki, T., Lee, T., Lee, J., & Ishii, M. (2006). Interfacial area concentration in boiling bubbly flow systems. *Chemical Engineering Science*, *61*, 7979.

Ishii, M., Kim, S., & Uhle, J. (2002). Interfacial area transport equation: model development and benchmark experiments. *International Journal of Heat and Mass Transfer*, *45*, 3111.

Issa, R. I. (1986). Solution of the implicitly discretized fluid flow equations by operator splitting. *Journal of Computational Physics*, *62*, 40.

Kim, D., & Ghajar, A. J. (2002). Heat transfer measurements and correlations for air–water flow of different flow patterns in a horizontal pipe. *Experimental Thermal and Fluid Science*, *25*, 659.

Knudsen, M. (1934). *The kinetic theory of gases. Some modern aspects*. London: Methuen and Co., Ltd.

Launder, B. E., & Spalding, D. B. (1972). *Lectures in mathematical models of turbulence*. London, England: Academic Press.

Lee, W. H. (1980). A pressure iteration scheme for two-phase flow modeling. In T. N. Veziroglu (Ed.), *Multiphase transport fundamentals, reactor safety, applications*. Washington, DC: Hemisphere Publishing.

Li, J. (1995). Calcul d'interface affiné par morceaux (piecewise linear interface calculation). *Comptes Rendus de l' Academie des Sciences Serie IIb, Paris*, *320*, 391.

Lide, D. R. (1998). *CRC handbook of chemistry and physics*. Boston: CRC Press.

Marek, R., & Straub, J. (2001). Analysis of the Evaporation Coefficient and the Condensation Coefficient of Water. *International Journal of Heat and Mass Transfer*, *44*, 39.

Mikami, S., Kobayashi, K., Ota, T., & Fujikawa, S. (2006). Molecular gas dynamics approaches to interfacial phenomena accompanied with condensation. *Experimental Thermal and Fluid Science*, *30*, 795.

Puckett, E. G. (1991). A volume-of-fluid interface tracking algorithm with applications to computing shock wave refraction. In H. Dwyer (Ed.), *Proceedings of the 4th International Symposium on Computational Fluid Dynamics* (p. 933).

Puckett, E. G., Almgren, A. S., Bell, J. B., Marcus, D. L., & Rider, W. J. (1997). A high-order projection method for tracking fluid interfaces in variable density incompressible flows. *Journal of Computational Physics*, *130*, 269.

Ranade, V. V. (2002). *Computational flow modeling for chemical reactor engineering* St Louis, Missouri, USA: Academic Press.

Son, G., & Dhir, V. K. (1998). Numerical simulation of film boiling near critical pressures with a level set method. *Journal of Heat Transfer*, *120*, 183.

Spalart, P., & Allmaras, S. (1992). *A one-equation turbulence model for aerodynamic flows* (Technical Report AIAA-92-0439). American Institute of Aeronautics and Astronautics.

Stefanidis, G. D., Heynderickx, G. J., & Marin, G. B. (2006). CFD simulations of steam cracking furnaces using detailed combustion mechanisms. *Computers and Chemical Engineering*, *30*, 635.

Thome, J. R. (2004). *Wolverine engineering data book III*. Wolverine Tube Inc.

Versteeg, H. K., & Malalasekera, W. (1995). *An introduction to computational fluid dynamics, the finite volume method*. Harlow, Essex, UK: Longman Scientific and Technical.

Wauters, S., & Marin, G. B. (2002). Kinetic modeling of coke formation during steam cracking. *Industrial & Engineering Chemistry Research*, *41*, 2379.

Welch, S. W. J., & Wilson, J. (2000). A volume of fluid based method for fluid flows with phase change. *Journal of Computational Physics*, *160*, 662.

Wilcox, D. C. (1998). *Turbulence modeling for CFD*. La Canada, CA: DCW Industries Inc.

Wu, H. L., Peng, X. F., Ye, P., & Eric Gong, Y. (2007). Simulation of refrigerant flow boiling in serpentine tubes. *International Journal of Heat and Mass Transfer*, *50*, 1186.

Xia, T., & Landman, U. (1994). Molecular evaporation and condensation of liquid *n*-alkane films. *Journal of Physical Chemistry*, *50*, 2498.

Yang, Z., Peng, X. F., & Ye, P. (2007). Numerical and experimental investigation of two phase flow during boiling in a coiled tube. *International Journal of Heat and Mass Transfer*, *50*, 1971.

Zaleski, S. (2003). *Computation of multiphase flow by volume of fluid and high-order front tracking methods*. Lecture given at short course: Modeling and computation of multiphase flows. Part IIb: Computational multi-fluid dynamics. Hosted by the Swiss Federal Institute of Technology, Zurich, Switzerland.

Zaleski, S. (2005). *Interface tracking—VOF*. Lecture given at course: Industrial two-phase flow CFD. Hosted by von Karman Institute for Fluid Dynamics, Belgium.